WILEY-VCH

DOI: 10.1002/adma.201702210
Article type: Communication

Ferroelectrics as smart mechanical materials

Kumara Cordero-Edwards, Neus Domingo, Amir Abdollahi, Jordi Sort, and Gustau Catalan**

K. Cordero-Edwards, Dr. N. Domingo, Prof. G. Catalan
Institut Català de Nanociencia i Nanotecnologia (ICN2), CSIC and The Barcelona Institute of Science and Technology (BIST), Campus UAB, Bellaterra, 08193 Barcelona, Spain

Email: kumara.cordero@icn2.cat , gustau.catalan@icn2.cat

Dr. A. Abdollahi
Laboratori de Càlcul Numèric (LaCàN), Universitat Politècnica de Catalunya (UPC), Campus Nord UPC-C2, E-08034 Barcelona, Spain

Prof. J. Sort
Departament de Física, Universitat Autònoma de Barcelona (UAB), Edifici Cc, E-0819 Bellaterra, Spain

Prof. J. Sort, Prof. G. Catalan
[3]Institució Catalana de Recerca i Estudis Avançats (ICREA), Pg. Lluís Companys 23, E-08010 Barcelona, Spain

Keywords: flexoelectricity, ferroelectricity, mechanical properties, ferroelectric memories, mechanical reading polarity.

The mechanical properties of homogeneous materials are insensitive to space inversion, even when they are crystallographically asymmetric. In practice, this means that turning a piezoelectric upside down or switching the polarization of a ferroelectric should not change its mechanical response. Strain gradients, however, introduce an additional source of asymmetry that has mechanical consequences. Using nanoindentation and contact-resonance force microscopy, we demonstrate that the mechanical response of an uniaxial ferroelectric ($LiNbO_3$) does change when its polarity is switched, and use this to quantify its flexoelectricity and to mechanically read the sign of its ferroelectric domains.

The mechanical properties of homogeneous materials (stiffness, hardness, toughness and so on) are insensitive to space inversion, because all the magnitudes involved (stress, strain, elastic constants) are described by even parity tensors. This mathematical argument is even valid for cristallographically asymmetric materials such as ferroelectrics and piezoelectrics, and physically, this means that the mechanical response of a ferroelectric material should not depend on whether its polar axis is pointing up or down. However, symmetry restrictions change when deformations are inhomogeneous.[1]-[4] For example, flexoelectricity (coupling between polarization and strain gradient) allows switching ferroelectric polarization by mechanical means, something that would be otherwise symmetry-forbidden if the strain was homogeneous.[5]-[6] Flexoelectricity can also affect the mechanical response.[7]-[9] Importantly, the incorporation of strain *gradients* (a third-rank tensor) breaks spatial inversion symmetry, so it allows asymmetric mechanical behaviour. In ferroelectrics, polarization also breaks inversion symmetry and may cooperate or compete with flexoelectricity. Thus, by switching ferroelectric polarization one can affect the total polarization, resulting in a material whose mechanical response to strain gradients can be switched with a voltage. By analogy with smart functional materials (materials whose functional response is sensitive to external input fields), ferroelectrics can be viewed as "smart mechanical materials", whose mechanical response to strain gradients can be switched with a voltage.

It is the purpose of this paper to demonstrate that the mechanical response of a ferroelectric is indeed switchable. We show that mechanical asymmetry not only affects toughness, as theoretically predicted,[10] but also all other mechanical properties, both plastic and elastic. This discovery, in turn, enables the use of purely mechanical means to quantify flexoelectricity, or to determine the sign of a ferroelectric domain (or, eventually, a ferroelectric memory bit) by just poking it. Both of these concepts are demonstrated here.

Physically, an asymmetric mechanical response can be rationalized by considering the energy cost of deforming a piezoelectric material that generates a polarization $\boldsymbol{P}$ in response to the deformation. This energy cost has two contributions: an elastic one, associated with the deformation itself (Hooke's law), and an electrostatic one, associated with the deformation-induced polarization. The electrostatic energy is $^1/_2 \chi^{-1} \boldsymbol{P}^2$, where χ the dielectric susceptibility is. Because the polarization is squared, the electrostatic energy is insensitive to its sign, so turning a piezoelectric crystal upside-down will not make it any softer. However, when the deformation is inhomogeneous, there are two sources of polarization: the strain itself, via piezoelectricity, and the strain gradient, via flexoelectricity. In a ferroelectric, which is a switchable piezoelectric, these two can be parallel or antiparallel depending on the ferroelectric polarity. Thus, the same inhomogeneous deformation will generate an enhanced polarization when piezoelectricity and flexoelectricity are parallel ($\boldsymbol{P} = \boldsymbol{P}_{piezo} + \boldsymbol{P}_{flexo}$) and a reduced polarization if they are antiparallel ($\boldsymbol{P} = -\boldsymbol{P}_{piezo} + \boldsymbol{P}_{flexo}$). The depolarization energy still depends on the square of the total polarization ($\boldsymbol{P}^2$), but the *magnitude* of $\boldsymbol{P}$ now depends on the sign of $\boldsymbol{P}_{\text{piezo}}$, so the cost of deformation becomes sensitive to polarity.

It is possible to investigate the mechanical response of ferroelectrics to inhomogeneous strain using nanoindentation, which generates flexoelectricity around a sharp indenter tip (Figure 1(a)). The samples studied are single crystals of Lithium Niobate ($LiNbO_3$). We have chosen this material because it is a uniaxial ferroelectric, meaning that only 180° domain switching is possible. This feature prevents any stress-induced ferroelastic reorientation of the polarization, [11] thus simplifying the analysis; however, the arguments used here can also be applied to thin films of ferroelastic-ferroelectrics such as $BaTiO_3$, $PbTiO_3$ or $BiFeO_3$, provided they are epitaxially constrained to have their polarization out-of-plane.

Depending on Li^+ concentration, $LiNbO_3$ can be stoichiometric or congruent. The latter has defect dipoles that can introduce an extrinsic asymmetry.[12]-[13] Here we have studied samples of both types: stoichiometric and congruent. The stoichiometric sample was single-domain (SLN), so space inversion was achieved by just splitting the crystal in two and turning one half upside-down. The congruent sample was periodically poled (PPLN), so both polarities were accessible on the same side. The results between SLN and PPLN were mutually consistent, indicating that sample stoichiometry or switching method do not affect the outcome.

Indentations were first performed in the monodomain crystal, z-cut (polarization perpendicular to the surface) and split with one half placed with polarization pointing up and the other pointing down. Both sides were equally polished to mirror-like appearance. In order to get statistically meaningful results, we performed and analyzed 50 indentations for each mechanical load (25 for each polarity) and measured applying 4 different maximum loads, i.e., a total of 200 indentations. Another set of 100 indentations (50 for each polarity) at a single load were performed on the PPLN. Further details of the nanoindentation measurements are provided in the Methods section, and the full dataset of raw results is provided in the Supporting Online Material.

Figure 1(b) is a schematic of the load-displacement (*F*-*h*) curve for a Berkovich indenter. During the loading process, the material undergoes both elastic and plastic deformation. The total energy related to this process is $U_T = \int_0^{h_{max}} F\, dh$, where h_{max} is the maximum depth reached during loading and *F* is the force applied by the indenter. The elastic deformation is recovered upon unloading; therefore, the elastic energy can be measured as $U_e = \int_{h_f}^{h_{max}} F\, dh$, where h_f is the final indentation depth after complete unloading. Subtracting the total and elastic energies results in the plastic energy $U_p = U_T - U_e$, see the inset in Figure 1(b).

We define asymmetry as $\%Asym \equiv 100\frac{\langle M^+\rangle - \langle M^-\rangle}{\langle M\rangle}$, where $\langle M^+\rangle - \langle M^-\rangle$ is the difference between the mean mechanical indentation energies of the up-polarized and down-polarized states, while $\langle M\rangle$ is the average for all polarities. Positive (negative) asymmetry indicates a larger value for the upward (downward) polarization. Figure 1(d) shows the asymmetry of the elastic, plastic, and total indentation energies as a function of the maximum indentation load. The total energy (elastic + plastic) is symmetric, reflecting that the mechanical energy provided by the indenter is independent of sample polarity, as it should. By contrast, asymmetry is observed for the plastic energy and thus also by the plasticity index (Figure 1S), which is the dimensionless parameter indicating the ratio of plastic energy to total energy, U_p / U_t. Since fracture toughness is proportional to plasticity index, [14],[15] crack propagation can be sensitive to the sign of polarization.[9],[10] The elastic energy (Figure 1(d)) is also asymmetric, and this implies that not only plastic but also elastic responses must be polarity-dependent. Using the Oliver-Pharr method,[16],[17] we have quantified one plastic and one elastic response: (a) hardness, as a measure of resistance to plastic deformation, and (b) contact stiffness, as a measure of the elastic response of the material. Both are found to depend on polarity (see Figure S1).

Having demonstrated that flexoelectricity induces mechanical asymmetry, we can use this asymmetry to quantify the flexoelectric coefficient of ferroelectrics. We do this for two reasons (i) to validate quantitatively that the flexoelectric origin of the mechanical asymmetry and (ii) to demonstrate that flexocoupling coefficients can be measured by mechanical means. In piezoelectrics, finding a new and reliable way to measure flexoelectricity is particularly important because the conventional methods (electromechanical rather than mechanical) yield unrealistically high results[3] due to piezoelectric contributions.[18], [19] We have derived a simplified analytical expression (see Supporting Online Material) relating the flexocoupling coefficient to the difference in free energy (ΔG) between the up and down polarized states:

$$f = \frac{1}{6}\frac{\bar{E}\Delta G}{P_0 F}, \qquad (1)$$

where P_0 is the ferroelectric spontaneous polarization (0.8 C/m^2 for $LiNbO_3$),[12] F is the maximum indentation load and $\bar{E}$ is the average of the elastic modulus measured for the up- and down-polarized states. Experimentally, the energy difference ΔG can be obtained by subtracting the measured elastic energy (area under the unloading curve in Figure 1(b)) of the upward and downward polar states, i.e. $\Delta G = U_e^+ - U_e^-$ .Using the values obtained experimentally at 7 mN, and Equation (1) the resulting flexocoupling coefficient f of SLN is 54 ± 4V, and for PPLN is 40 ± 5V.

The obtained flexocoupling coefficients are still somewhat larger than the Kogan-Tagantsev expectation value f <10V,[1]-[3] but the order-of-magnitude agreement is nevertheless remarkable considering the simplifications made in order to obtain the analytical expression in eq. (1) (see Supporting Online Material). The accuracy also represents an enormous improvement compared to beam-bending experiments, which for ferroelectrics always yield flexocoupling coefficients that are many orders of magnitude too large.[3]

Another notable consequence of these results is that they allow determining the polarity of a ferroelectric just by indenting its surface. This is demonstrated by contact stiffness measurements performed on PPLN (Figure 2), which show that downward polarized material is stiffer while the upward-oriented one is more flexible.

Nanoindentation is, by definition, a destructive method, but since stiffness is an elastic property it is not necessary to punch holes in order to read polarity. To prove this point, we use Contact Resonance Force Microscopy (CRFM)[20] (see Methods): with this technique, we deliver an oscillatory force by vibrating the AFM in hard contact with the surface of the ferroelectric. The vibration amplitude peaks when the vibration frequency delivered by the cantilever coincides with the mechanical resonance frequency of the tip-sample contact.

Since contact resonance frequency depends on tip-sample mechanical coupling, it is sensitive to the material's stiffness, with higher resonance frequency corresponding to higher stiffness. The sensitivity has been used in the past to evidence contrast in Young's Modulus between domains of different ferroelastic orientation,[21]-[22] but the technique was thought to be blind with respect to polarization sign. Our results, however, show that there is a measurable difference between the contact resonance frequency of oppositely-polarized domains (Figure 3), with down-polarized domains resonating at higher frequencies (stiffer) than up-polarized ones, in agreement with the nanoindentation results. This result is explained by the same arguments as in the indentation experiment: inhomogeneous deformation under the AFM tip induces a flexoelectric polarization that either adds to or subtracts from the piezoelectricity of the domains depending on their ferroelectric sign, resulting in asymmetric energy costs of deformation and thus different stiffness and contact resonance frequency. These results thus evidence the importance of tip-induced gradient effects for tip-sample coupling in AFM, and demonstrate that such gradient effects can be exploited to mechanically read polarity.

To summarize: the results indicate that the mechanical responses (plastic and elastic) of a ferroelectric to inhomogeneous deformation are asymmetric and switchable. This switchable asymmetry was used both to quantify the flexoelectric coefficient itself and to determine the polar sign of a ferroelectric domain by purely mechanical means. This demonstration opens up new device possibilities such reading a ferroelectric memory without electrodes, or making coatings whose mechanical response to localized deformations (e.g. scratching) can be modified with a voltage. Nowadays ferroelectrics are already considered as smart multifunctional materials on account their switchable polarization and electromechanical response. Our results show that they can also be considered as smart mechanical materials.

Experimental Section

Sample preparation and characterization: Depending on the growth process, single crystals can be *stoichiometric*, with a ratio of 1: 1: 3 for Li^{+}: Nb^{+5}: O^{-2}, or (the most common) *congruent* which exhibit Li^{+} deficiency. Such lithium vacancies can result in defect dipoles that may be either parallel or antiparallel to the ferroelectric polarization, thus introducing an additional and extrinsic source of asymmetry [12]-[13] that can complicate the analysis of the results. To guarantee that any evidence of asymmetry originates from flexoelectricity, we use Stoichiometric Lithium Niobate (SLN) single crystals, purchased from MTI Corporation. These are single-domain, so the SLN z-cut single crystal was cut in two equal pieces and we turned one upside-down in order to study two areas with opposite polarization. Both crystals were chemical cleaned. They were sonicated for 15 min in acetone, isopropanol and MilliQ water sequentially. Finally, both were glued in a metallic disc with silver paste, one with the polarization pointing upward and the other downward. We also studied a periodically-poled lithium niobate (PPLN) crystal provided by Asylum Research, Santa Barbara, CA., and chemically cleaned like the SLN. These crystals were congruent; there are no commercially available stoichiometric crystals of PPLN. The polarization of the samples was checked by Piezoresponse Force Microscopy (PFM) using an MFP-3D AFM from Asylum Research, Santa Barbara, CA.

Nanoindentation: Experiments were carried out in the load-control mode, using a UMIS instrument from Fischer-Cripps Laboratories equipped with a Berkovich pyramidal-shaped diamond tip. The thermal drift was always kept below ± 0.05 nms^{-1}. Four different loads (7 mN, 10 mN, 15 mN and 20 mN) were applied. To ensure statistical robustness and accuracy of the results a total of 50 indents per load (25 in each polar state, see Figure 1c)) were performed in the SLN single crystal, and a total of 100 indents per load in the PPLN single

crystal. Indents were spaced 15 μm apart (see Figure 1c)), ensuring a sufficient independence of the indents in all cases.

PFM images on PPLN: To correlate the direction of the polarization with each indentation, PFM experiments were carried out, using an MFP-3D AFM, and OMCL – AC240TM – R3 cantilevers, with a k ~ 2 N/m. PFM was mainly operated in DART mode to benefit from resonance signal enhancement; in PFM, an electrical *ac* signal is applied to the tip used as top electrode that excites the sample and mechanical response due to inverse piezoelectric effect is monitored.

CRFM images on PPLN: Experiments were carried out using an MFP-3D AFM, in a controlled ambient with N_2. In CRFM a mechanical *ac* excitation signal is applied to the cantilever in contact with the surface, and the resonance frequency is monitored, in this case also operating in DART mode. The mechanical resonance of the cantilever in contact with the surface strongly depends on the coupling with the mechanical properties of the surface. Nanosensors NCL Pt coated tips, with k ~ 48 N/m were used. The contact force between the cantilever and the sample was about 25 μN.

Supporting Information

Supporting Information is available from the Wiley Online Library or from the author.

Acknowledgements

K. C-E and G.C. acknowledges ERC Starting Grant 308023. Financial support has been obtained under projects from the Spanish Ministerio de Economía y Competitividad (MINECO) under projects FIS2013-48668-C2-1-P and FIS2015-73932-JIN, and the MAT2014-57960-C3-1-R cofinanced by the 'Fondo Europeo de Desarrollo Regional' (FEDER). ICN2 acknowledges support from the Severo Ochoa Program (MINECO, Grant SEV-2013-0295). This work has also been partially funded by 2014-SGR-1015 and 2014-SGR-1216 projects from the Generalitat de Catalunya.

Received: ((will be filled in by the editorial staff))
Revised: ((will be filled in by the editorial staff))
Published online: ((will be filled in by the editorial staff))

References

[1] S. Kogan, *Sov. Phys. Solid State* **1964**, 5, 2069-2079.

[2] A. K. Tagantsev. *Phys. Rev. B* **1986,** 34, 5883.

[3] P. Zubko, G. Catalán, A.K. Tagantsev. *Annu. Rev. Mater. Res.* **2013**, 43: 387 – 421.

[4] R. S. Lakes, R.L. Benedict. *Int. J. Engng Sci.* **1982,** 29, 1161.

[5] H. Lu, C. –W. Bark, D. Esque de los Ojos, J. Alcalá, C. B. Eom, G. Catalán, A. Gruverman. *Science* **2012,** 336, 59.

[6] J. Ocenásek, H. Lu, C. W. Bark, C. B Eom, J. Alcalá, G. Catalan, A. Gruverman. *Phys. Rev B.* **2015**, 92, 035417.

[7] M. Gharbi, Z.H. Sun, P. Sharma, K. White. *Appl. Phys. Lett.* **2009,** 95, 142901.

[8] C.R. Robinson, K.W. White, P. Sharma. *Appl. Phys. Lett* **2012,** 101, 122901.

[9] H. Zhou, Y. Pei, F. Li, H. Luo, D. Fang. *Appl. Phys. Lett* **2014,** 104, 061904.

[10] A. Abdollahi, C. Peco, D. Millán, M. Arroyo, G. Catalán, I. Arias. *Phys. Rev B* **2015,** 92, 094101.

[11] M.J. Reece, F. Guiu. *Philosophical Magazine A* **2002,** 82, 1: 29-38.

[12] S. Kim, V. Gopalan, K. Kitamura, Y. Furukawa. Y. *J. Appl. Phys* **2001,** 90, 2949.

[13] V. Gopalan, V. Dierolf, D.A. Scrymgeour. *Annu. Rev. Mater. Res* **2007,** 37, 449 – 489.

[14] G.M. Pharr. *Mater. Sci. Eng. A* **1998,** 253, 151-159.

[15] Y. –T- Cheng, C. –M. Cheng. *Appl. Phys. Lett.* **1998,** 73, 614 – 616.

[16] W.C. Oliver, G.M. Pharr. *J. Mater. Res.* **1992,** 7, 1564 – 1583.

[17] Fisher – Cripps, A.C. Nanoindentation. **2002,** 3rd *Ed. Springer – Verlag*, New York.

[18] J. Narvaez, S. Saremi, J. Hong, M. Stengel, G. Catalan. *Phys. Rev. Lett.* **2015,** 115, 037601.

[19] A. Biancoli, C.M. Fancher, J.L. Jones, D. Damjanovic, D. *Nat. Mat.* **2015,** 14, 224–229 .

[20] U. Rabe, S. Amelio, E. Kester, V. Scherer, S. Hirsekorn, W. Arnold, *Ultrasonics* **2000,** 38, 430-437.

[21] U. Rabe, M. Kopycinska, S. Hirsekorn, J. Muñoz-Saldaña, G.A. Schneider, W. Arnold, *J. Phys. D: Appl. Phys.* **2002,** 35, 2621–2635.

[22] X. L. Zhou, F.X. Li, H.R Zeng, H. R. *J. Appl. Phys.* **2013,** 113, 187214.

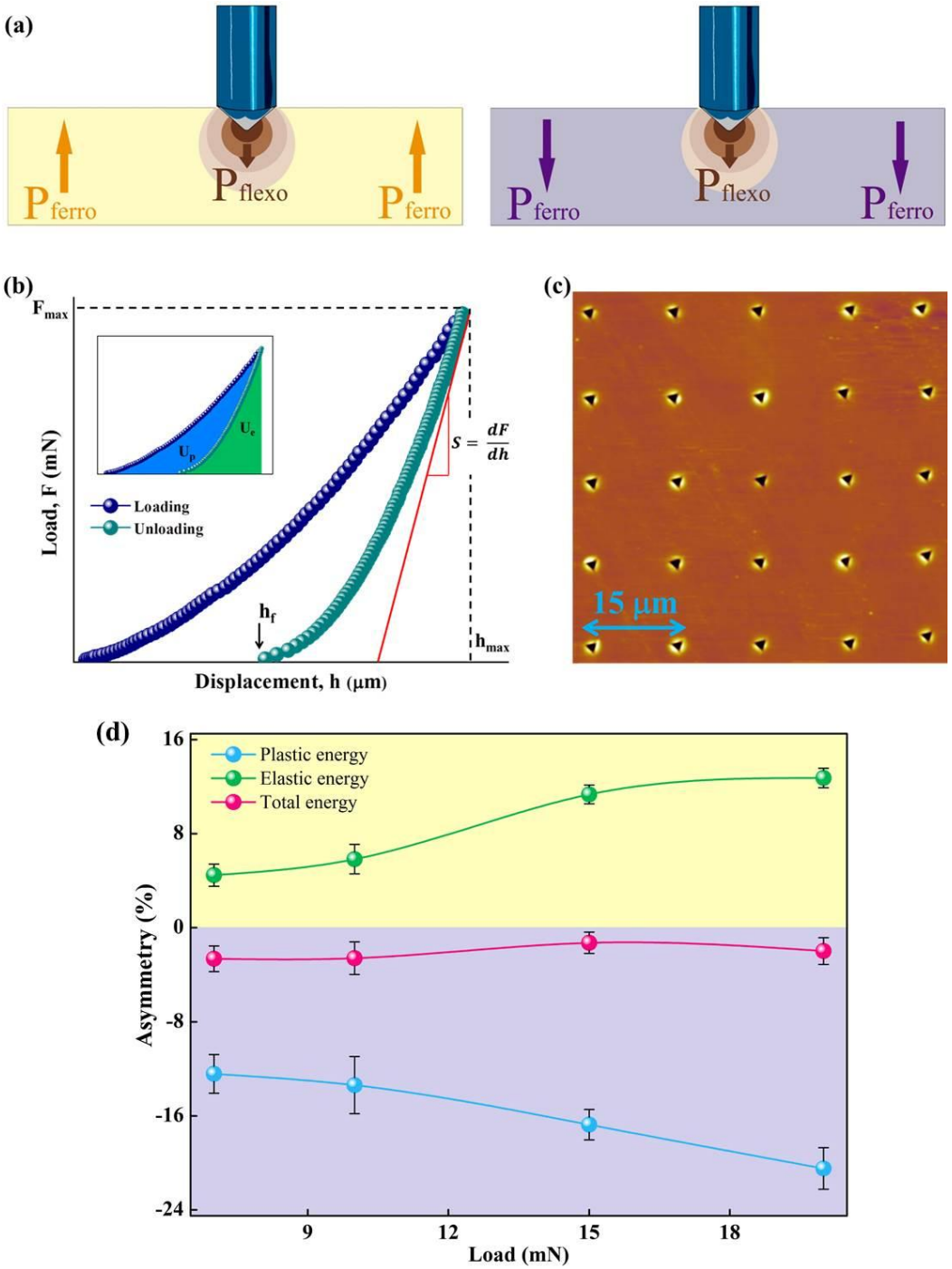

Figure 1: (a) Schematic of the strain gradient field and the associated polarizations (arrows) induced by the indenter tip on a uniaxial ferroelectric with polarization pointing up (left), and polarization pointing down (right). (b) Schematic of the loading and unloading force-displacement curve performed by the nanoindenter, from which the energies (inset), and mechanical parameters are obtained. (c) AFM topography image of the surface of an SLN crystal after performing 25 nanoindentations with the same indentation force. (d) Asymmetry behavior of energies as a function of the maximum indentation load in SLN single crystals, showing that both plastic and elastic mechanical responses are asymmetric.

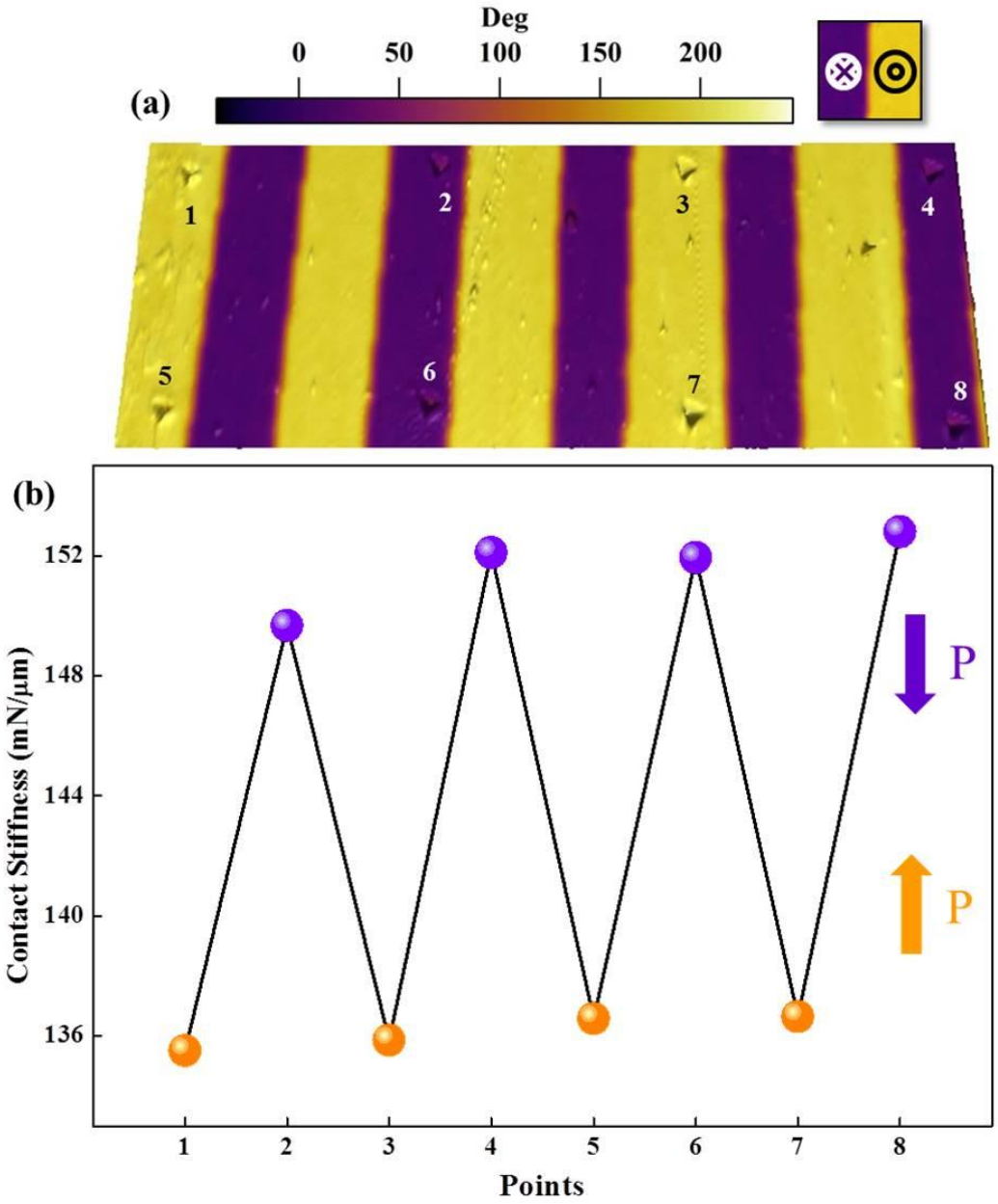

Figure 2: a) 3D plot of topography with superimposed PFM phase image of a few indents performed in PPLN at 7 mN. Yellow means that the polarization is pointing up, whereas purple means that it is pointing down. b) Contact Stiffness measured as a function of the number of indent in (a), showing that the relative stiffness is a direct indicator of a polar state, and therefore it is possible to "read" the polarization of a ferroelectric from its mechanical response.

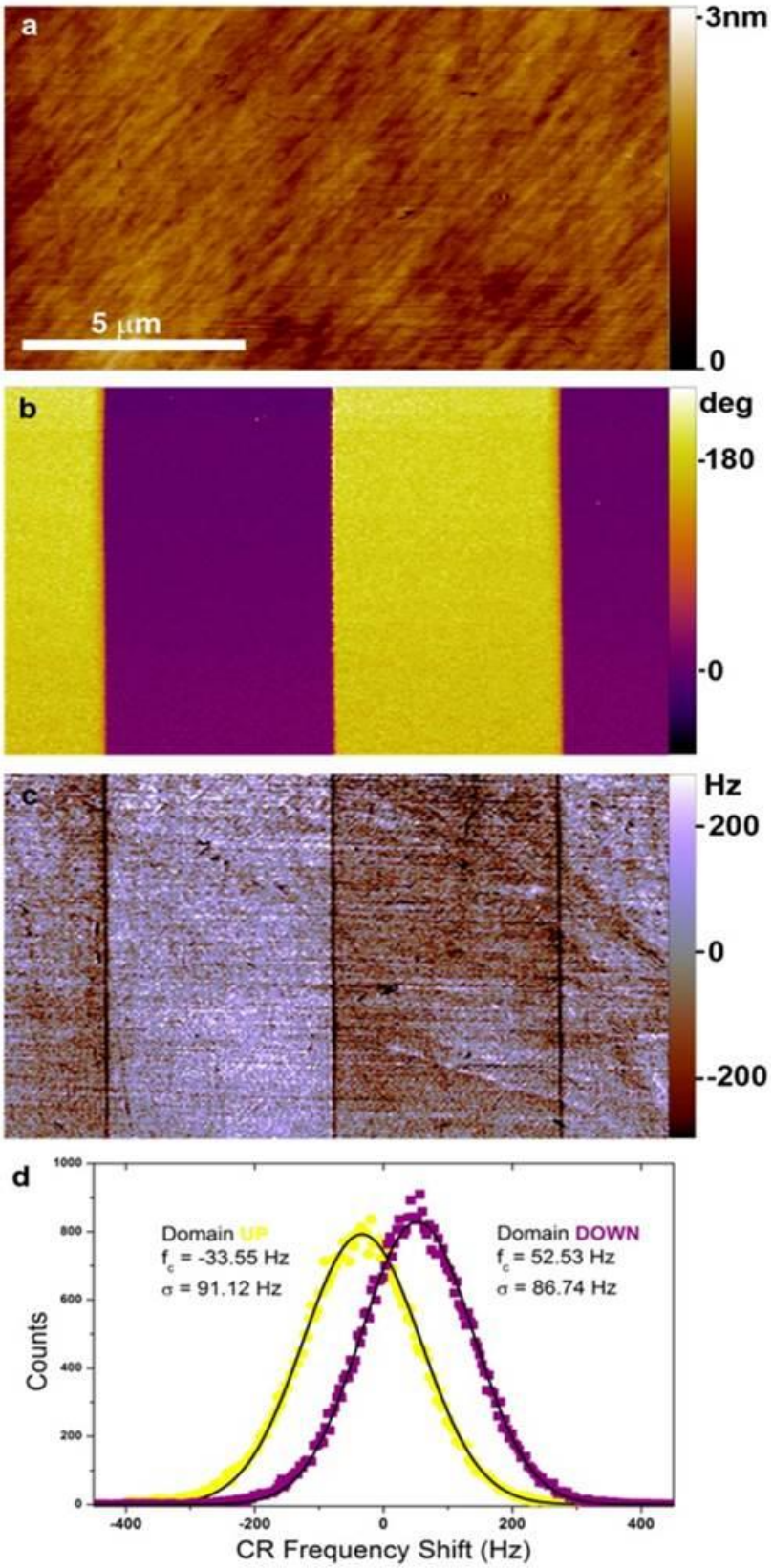

Figure 3: **a**. Topography and **b.** Phase PFM image showing the polarization of the domains in a periodically pooled $LiNbO_3$ sample (PPLN), with Ph_{PFM} = 0º for domains pointing down and Ph_{PFM} = 180º for domains pointing up. **c.** Contact resonance frequency mapping of the PPLN surface, the contact resonance frequency is shifted towards higher frequencies for down-polarized domains, meaning they are stiffer, and to lower frequencies for the up-

polarized domains, meaning they are softer. **d.** Histogram of the CR-AFM image shown in **c**: the yellow dots correspond to the frequency shift counts in the areas associated to domains pointing up and purple squares to domains pointing down. Black lines are the corresponding Gaussian fittings, with parameters shown in the inset. The total CR frequency contrast among different polarized domains is of about $\Delta f \sim 86$ Hz, using a cantilever of $k \sim 48$ N/m.

The table of contents

Ferroelectrics are smart multifunctional materials: their polarization responds to external stimuli (stress, voltage, temperature) for transductors, and can be switched for memories. Here, we show that, thanks to flexoelectricity, their mechanical response to strain gradients is switchable, so that they may also be regarded as mechanically smart. Two practical consequences, demonstrated here, are mechanical measurement of flexoelectricity and mechanical reading of ferroelectric sign.

Keyword mechanical reading polarity

K. Cordero-Edwards*, N. Domingo, A. Abdollahi, J. Sort, and G. Catalan*

Ferroelectrics as smart mechanical materials

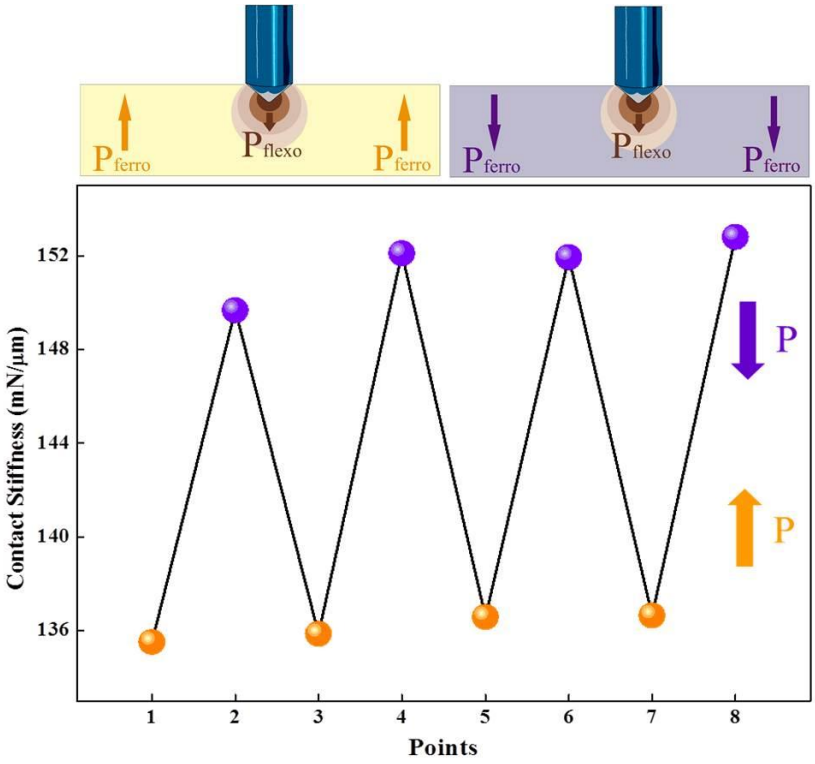

Supporting Information

Ferroelectrics as smart mechanical materials

Kumara Cordero-Edwards, Neus Domingo, Amir Abdollahi, Jordi Sort, and Gustau Catalan**

1. Asymmetry behavior

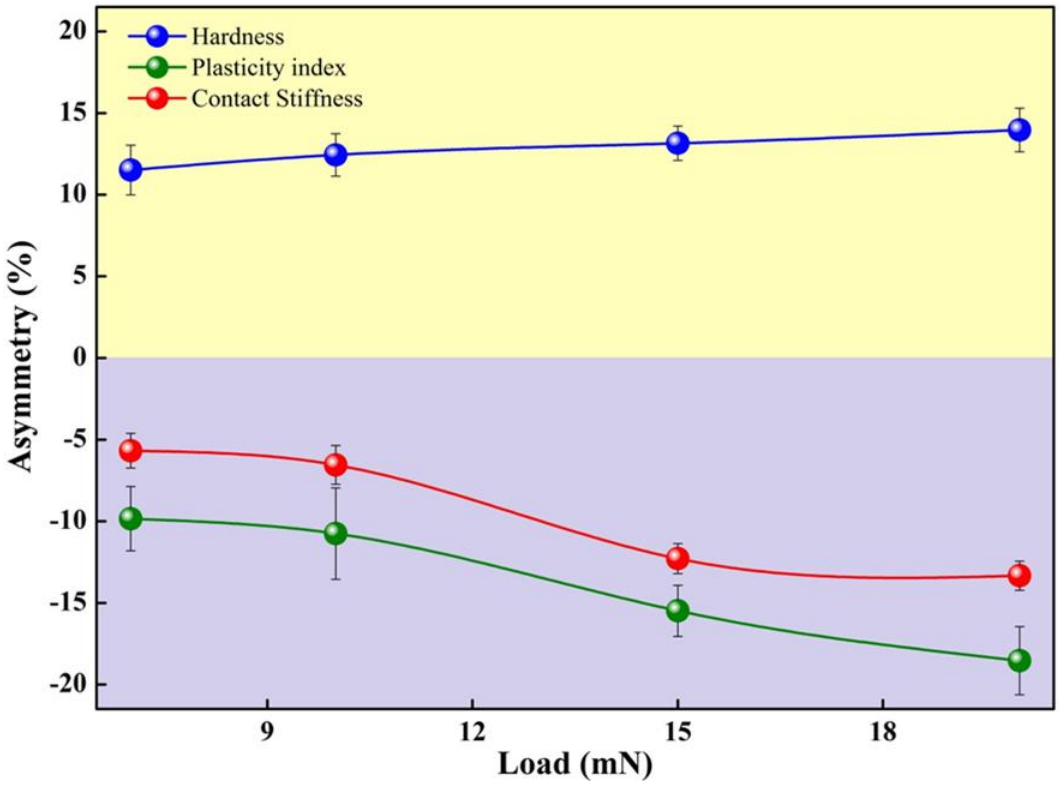

Figure S1: Asymmetry behavior of mechanical properties as a function of the maximum indentation load in SLN single crystals.

2. Nanomechanics: measuring flexoelectricity from nanoindentation

The role of flexoelectricity on the response of ferroelectrics can be exposed by their free energy [[9]-[9]]:

$$G = \int \left[\frac{1}{2}\alpha_{ij} P_i P_j + \frac{1}{4}\beta_{ijkl} P_i P_j P_k P_l + \frac{1}{6}\gamma_{ijklmn} P_i P_j P_k P_l P_m P_n + \frac{1}{2} c_{ijkl} \varepsilon_{ij} \varepsilon_{kl} - \frac{1}{2} q_{ijkl} \varepsilon_{ij} P_k P_l + 12 g_{ijkl} P_{i,j} P_k P_l - f_{ijkl} P_k \partial \varepsilon_{ij} \partial x_l dV, \quad (1)$$

where the first three terms represent the Landau free energy density with the phenomenological Landau-Devonshire coefficients [[3]], P_i is the polarization, and ε_{ij} is the strain. The fourth term denotes the elastic energy density of the system and c_{ijkl} is the elastic tensor. The fifth term indicates the coupling between the polarization and strain, where q_{ijkl} is the electrostrictive tensor. The sixth term is the polarization gradient energy density and g_{ijkl} is the correlation energy tensor.

The last term in Equation 1 is the flexoelectric coupling energy density, and f_{ijkl} is the flexocoupling tensor describing both direct and converse flexoelectric effects [[3], [5]]. We can use this equation to calculate the energy difference between the positively (P^+) and negatively (P^-) polarized states in the presence of a strain gradient. All terms with even powers of polarization remain identical under polar inversion and therefore disappear from the subtraction, leaving the free energy difference as:

$$\Delta G = G^+ - G^- = \int \left[f_{ijkl} P_k^- \frac{\partial \varepsilon_{ij}}{\partial x_l} - f_{ijkl} P_k^+ \frac{\partial \varepsilon_{ij}}{\partial x_l} \right] dV. \quad (2)$$

Equation 1 and 2 show explicitly that flexoelectricity introduces a difference (bias) into the otherwise symmetric ferroelectric double well.

Considering that $P_k^+ = -P_k^- \equiv P_k$, Equation 2 can be simplified to:

$$\Delta G = -2 \int f_{ijkl} P_k \frac{\partial \varepsilon_{ij}}{\partial x_l} dV. \quad (3)$$

Starting from Equation 3, and considering an isotropic medium, the non-zero independent flexoelectric coefficients f_{ijkl} reduce to two which are the longitudinal f_{11} and transversal f_{12} flexoelectric coefficients [[6]]. By assuming that $f_{11} = f_{12} = f$, we can expand the right-hand side of Equation 3 as

$$\Delta G = -2 \int \begin{matrix} f\left(P_1 \frac{\partial \varepsilon_{11}}{\partial x_1} + P_2 \frac{\partial \varepsilon_{22}}{\partial x_2} + P_3 \frac{\partial \varepsilon_{33}}{\partial x_3}\right) \\ + f\left(P_1 \frac{\partial \varepsilon_{22}}{\partial x_1} + P_1 \frac{\partial \varepsilon_{33}}{\partial x_1} + P_2 \frac{\partial \varepsilon_{11}}{\partial x_2} + P_2 \frac{\partial \varepsilon_{33}}{\partial x_2} + P_3 \frac{\partial \varepsilon_{11}}{\partial x_3} + P_3 \frac{\partial \varepsilon_{22}}{\partial x_3}\right). \end{matrix} dV \quad (4)$$

Considering x_3 as the uniaxial direction of the polarization, i.e. $P_1 = P_2 = 0$, and using Hook's law, $\varepsilon = \sigma/E$, Equation (4) converts to

$$\Delta G = -\frac{2fP_0}{E}\int\left(\frac{\partial\sigma_{11}}{\partial x_3} + \frac{\partial\sigma_{22}}{\partial x_3} + \frac{\partial\sigma_{33}}{\partial x_3}\right) dV, \qquad (5)$$

where P_0 is the spontaneous polarization of $LiNbO_3$.

Following an idealized model of indentation [[7]], the surface of the indenter is assumed to be encased in a semi-cylindrical or hemispherical core where there is a hydrostatic stress. The hydrostatic stress can thus be written as $\hat{\sigma} = (\sigma_{11} + \sigma_{22} + \sigma_{33})/3$, and the volume integral can be reduced over the surface as

$$\Delta G = -\frac{6fP_0}{E}\iint \hat{\sigma}\ dx_1 dx_2\ , \qquad (6)$$

The stress is $\hat{\sigma} = -F/A$, with F being the indentation force and A the projected area of the elastic contact; Equation 6 therefore can be written as

$$\Delta G = \frac{6fFP_0}{E}\ . \qquad (7)$$

And thus, the flexocoupling coefficient f is obtained as

$$f = \frac{1}{6}\frac{E\Delta G}{P_0 F}. \qquad (8)$$

where P_0 is the spontaneous polarization, F is the maximum indentation load and $\bar{E}$ is the average of the elastic modulus measured for the up- and down-polarized states.

3. Full dataset of the raw results.

Table 2S1: Data of SLN at 20 mN.

Polarization	Upward	Upward	Upward	Upward	Upward	Downward	Downward	Downward	Downward	Downward
Property	Hardness	Contact Stiffness	Plastic energy	Elastic energy	Total energy	Hardness	Contact Stiffness	Plastic energy	Elastic energy	Total energy
Units	GPa	mN/µm	nJ	nJ	nJ	GPa	mN/µm	nJ	nJ	nJ
1	11,752	192,056	1,006	1,440	2,446	10,341	226,202	1,192	1,250	2,443
2	11,403	194,497	1,036	1,435	2,470	9,678	225,350	1,223	1,283	2,507
3	13,543	172,647	0,777	1,633	2,411	10,087	210,315	1,196	1,305	2,501
4	10,475	198,356	1,147	1,405	2,552	9,915	222,163	1,214	1,271	2,485
5	12,151	188,545	0,959	1,471	2,430	10,094	218,708	1,172	1,269	2,441
6	12,465	178,021	0,903	1,542	2,445	10,096	217,117	1,204	1,302	2,505
7	11,161	195,336	1,019	1,444	2,462	9,823	223,407	1,249	1,267	2,516
8	11,629	196,885	0,961	1,454	2,415	10,291	216,104	1,185	1,295	2,481
9	11,584	189,569	0,951	1,480	2,431	9,870	225,795	1,240	1,268	2,508
10	10,726	189,684	1,106	1,462	2,568	9,928	221,348	1,272	1,272	2,544
11	10,568	203,513	1,067	1,409	2,476	10,864	210,678	1,089	1,335	2,424
12	11,624	188,125	0,967	1,484	2,451	10,137	216,430	1,211	1,299	2,510
13	11,200	196,563	1,049	1,437	2,486	9,874	227,553	1,244	1,250	2,494
14	11,464	193,235	1,026	1,415	2,441	9,782	225,216	1,236	1,263	2,499
15	11,389	195,052	0,995	1,435	2,430	10,182	218,732	1,187	1,282	2,468
16	11,859	194,569	0,907	1,478	2,386	10,180	219,187	1,235	1,293	2,529
17	11,850	192,679	0,956	1,452	2,408	10,079	224,258	1,180	1,275	2,455
18	12,001	189,463	0,911	1,481	2,392	9,485	230,833	1,325	1,229	2,554
19	11,129	197,929	1,046	1,435	2,482	10,540	209,041	1,139	1,316	2,455
20	11,601	201,389	0,968	1,441	2,409	10,235	219,079	1,207	1,277	2,484
21	12,166	189,412	0,890	1,472	2,361	9,342	233,409	1,318	1,235	2,553
22	11,525	191,415	0,968	1,445	2,413	9,651	218,668	1,268	1,294	2,562
23	11,355	200,279	1,024	1,398	2,423	10,535	213,393	1,126	1,337	2,463
24	12,034	190,025	0,909	1,501	2,410	10,954	209,371	1,073	1,373	2,445
25	11,508	194,437	0,987	1,463	2,449	10,321	218,615	1,146	1,302	2,448

Table 2S2: Data of SLN at 15 mN.

Polarization	Upward	Upward	Upward	Upward	Upward	Downward	Downward	Downward	Downward	Downward
Property	Hardness	Contact Stiffness	Plastic energy	Elastic energy	Total energy	Hardness	Contact Stiffness	Plastic energy	Elastic energy	Total energy
Units	GPa	mN/µm	nJ	nJ	nJ	GPa	mN/µm	nJ	nJ	nJ
1	12,001	163,999	0,663	0,924	1,587	10,600	194,336	0,736	0,801	1,537
2	11,385	162,409	0,660	0,952	1,611	10,196	197,152	0,753	0,808	1,560
3	11,778	173,440	0,670	0,888	1,559	9,855	188,069	0,776	0,878	1,653
4	12,102	169,698	0,621	0,914	1,535	10,206	192,441	0,753	0,810	1,564
5	12,506	162,703	0,596	0,945	1,542	10,000	199,278	0,813	0,782	1,595
6	10,934	176,849	0,713	0,892	1,606	9,641	209,635	0,828	0,786	1,613
7	12,376	167,828	0,590	0,945	1,534	10,934	185,795	0,696	0,853	1,550
8	11,179	177,457	0,675	0,895	1,571	10,666	183,721	0,730	0,845	1,576
9	11,880	164,312	0,646	0,910	1,556	10,159	192,738	0,777	0,814	1,591
10	11,846	168,800	0,627	0,937	1,564	10,530	192,482	0,734	0,836	1,569
11	11,592	172,596	0,656	0,913	1,569	10,338	190,327	0,747	0,836	1,583
12	11,395	169,657	0,657	0,905	1,562	10,191	199,538	0,806	0,793	1,598
13	11,510	172,852	0,677	0,895	1,571	10,523	182,148	0,726	0,853	1,578
14	11,411	177,093	0,678	0,887	1,565	10,104	198,092	0,788	0,801	1,589
15	11,613	172,275	0,645	0,902	1,547	10,324	190,973	0,770	0,814	1,584
16	13,071	162,012	0,546	0,968	1,515	10,330	191,481	0,774	0,815	1,589
17	10,910	186,706	0,685	0,860	1,545	10,026	194,188	0,790	0,816	1,606
18	11,958	174,743	0,644	0,897	1,541	10,433	194,702	0,761	0,803	1,563
19	11,282	176,548	0,651	0,904	1,555	10,356	195,886	0,752	0,809	1,562
20	11,552	173,027	0,683	0,900	1,583	10,355	195,335	0,775	0,818	1,594
21	11,965	163,942	0,646	0,948	1,594	9,979	197,911	0,793	0,800	1,593
22	12,024	168,963	0,638	0,921	1,560	10,742	192,097	0,749	0,828	1,576
23	12,369	168,613	0,605	0,930	1,535	10,294	190,181	0,755	0,815	1,570
24	11,178	180,799	0,672	0,885	1,557	10,081	201,823	0,790	0,775	1,564
25	11,996	172,929	0,638	0,927	1,565	10,700	190,307	0,770	0,805	1,575

Table 2S3: Data of SLN at 10 mN.

Polarization	Upward	Upward	Upward	Upward	Upward	Downward	Downward	Downward	Downward	Downward
Property	Hardness	Contact Stiffness	Plastic energy	Elastic energy	Total energy	Hardness	Contact Stiffness	Plastic energy	Elastic energy	Total energy
Units	GPa	mN/µm	nJ	nJ	nJ	GPa	mN/µm	nJ	nJ	nJ
1	12,431	145,385	0,346	0,470	0,816	11,921	127,538	0,222	0,567	0,789
2	11,478	148,279	0,379	0,467	0,845	11,791	160,557	0,360	0,424	0,784
3	11,933	139,480	0,359	0,490	0,849	11,017	160,989	0,385	0,432	0,817
4	11,922	143,935	0,346	0,484	0,830	10,548	160,362	0,434	0,425	0,859
5	12,071	144,321	0,361	0,469	0,830	10,907	154,533	0,390	0,443	0,833
6	11,877	147,014	0,343	0,472	0,815	11,378	147,944	0,377	0,452	0,829
7	13,428	136,607	0,315	0,491	0,806	10,790	147,055	0,392	0,454	0,846
8	13,348	136,957	0,302	0,494	0,796	10,842	154,114	0,388	0,445	0,834
9	12,589	141,085	0,339	0,477	0,816	11,036	150,941	0,393	0,462	0,856
10	11,953	146,644	0,349	0,475	0,825	10,456	158,281	0,412	0,441	0,853
11	12,740	143,148	0,325	0,475	0,801	10,986	155,164	0,383	0,453	0,837
12	11,900	145,102	0,360	0,474	0,834	10,454	161,384	0,421	0,426	0,848
13	12,219	144,097	0,330	0,476	0,806	11,985	141,094	0,357	0,461	0,819
14	12,490	141,871	0,329	0,483	0,812	11,337	151,634	0,380	0,450	0,830
15	12,419	145,231	0,334	0,480	0,814	10,163	162,240	0,415	0,437	0,852
16	14,243	137,737	0,270	0,513	0,783	10,452	155,013	0,400	0,445	0,845
17	12,333	138,936	0,354	0,484	0,838	11,412	150,910	0,375	0,455	0,831
18	12,669	143,893	0,338	0,465	0,803	10,748	154,230	0,400	0,445	0,845
19	12,884	142,870	0,322	0,487	0,809	10,935	155,900	0,399	0,452	0,851
20	11,807	148,930	0,355	0,466	0,821	11,380	150,086	0,374	0,455	0,829
21	12,816	144,874	0,318	0,474	0,791	10,486	165,828	0,407	0,429	0,836
22	12,023	150,711	0,358	0,461	0,819	10,580	148,512	0,377	0,461	0,838
23	12,269	145,013	0,343	0,477	0,820	11,101	152,827	0,390	0,459	0,848
24	12,056	150,027	0,341	0,458	0,799	11,118	148,367	0,397	0,460	0,857
25	12,738	145,160	0,321	0,473	0,794	10,444	165,368	0,417	0,426	0,842

Table 2S4: Data of SLN at 7 mN.

Polarization	Upward	Upward	Upward	Upward	Upward	Downward	Downward	Downward	Downward	Downward
Property	Hardness	Contact Stiffness	Plastic energy	Elastic energy	Total energy	Hardness	Contact Stiffness	Plastic energy	Elastic energy	Total energy
Units	GPa	mN/µm	nJ	nJ	nJ	GPa	mN/µm	nJ	nJ	nJ
1	12,735	126,621	0,197	0,267	0,463	12,901	130,945	0,222	0,248	0,470
2	13,278	118,582	0,182	0,279	0,461	11,911	118,717	0,205	0,277	0,483
3	12,655	119,013	0,196	0,276	0,472	11,062	130,169	0,220	0,260	0,479
4	12,645	120,772	0,188	0,280	0,468	11,941	117,123	0,205	0,282	0,486
5	13,368	120,187	0,185	0,274	0,460	11,652	129,079	0,203	0,266	0,469
6	12,283	125,358	0,202	0,270	0,472	12,147	125,128	0,200	0,272	0,472
7	12,847	119,062	0,187	0,277	0,464	8,719	118,718	0,209	0,280	0,489
8	13,477	113,793	0,188	0,280	0,467	11,392	132,841	0,215	0,258	0,473
9	12,179	125,287	0,205	0,260	0,465	11,616	126,065	0,205	0,268	0,473
10	13,304	115,695	0,181	0,285	0,467	11,888	124,038	0,208	0,268	0,476
11	12,303	120,601	0,204	0,269	0,474	10,987	128,637	0,238	0,257	0,495
12	13,937	113,795	0,159	0,295	0,455	12,569	121,063	0,194	0,274	0,468
13	12,831	117,681	0,195	0,282	0,477	11,638	127,355	0,208	0,264	0,472
14	13,755	119,058	0,179	0,277	0,456	12,149	126,621	0,198	0,265	0,463
15	12,960	122,723	0,193	0,268	0,461	11,906	129,819	0,213	0,260	0,473
16	13,631	123,402	0,170	0,276	0,446	11,966	125,447	0,198	0,271	0,470
17	13,897	119,838	0,169	0,277	0,446	11,314	125,828	0,212	0,269	0,481
18	12,866	117,559	0,199	0,281	0,479	12,012	117,272	0,205	0,278	0,483
19	13,808	114,979	0,183	0,285	0,468	11,779	128,184	0,211	0,263	0,474
20	12,889	123,703	0,190	0,268	0,458	12,266	120,868	0,203	0,273	0,476
21	14,203	110,906	0,158	0,299	0,457	11,635	127,951	0,205	0,269	0,473
22	13,886	118,674	0,170	0,288	0,457	11,983	128,037	0,203	0,263	0,466
23	13,235	118,618	0,182	0,277	0,459	12,190	126,422	0,208	0,264	0,471
24	12,425	122,340	0,191	0,270	0,461	12,300	140,134	0,225	0,246	0,471
25	13,273	117,248	0,172	0,287	0,459	10,971	133,556	0,227	0,250	0,477

Table 2S5: Data of PPLN at 7 mN.

Polarization	Upward	Upward	Upward	Upward	Upward	Downward	Downwar	Downward	Downward	Downward
Property	Hardness	Contact Stiffness	Plastic energy	Elastic energy	Total energy	Hardness	Contact Stiffness	Plastic energy	Elastic energy	Total energy
Units	GPa	mN/µm	nJ	nJ	nJ	GPa	mN/µm	nJ	nJ	nJ
1	12,701	142,265	0,231	0,246	0,477	12,049	149,684	0,243	0,231	0,474
2	12,540	138,653	0,232	0,251	0,483	11,915	152,115	0,246	0,233	0,479
3	13,226	137,928	0,220	0,247	0,467	13,231	143,113	0,213	0,251	0,464
4	12,796	136,577	0,232	0,251	0,482	11,814	147,557	0,250	0,233	0,483
5	12,327	138,788	0,243	0,237	0,480	12,361	145,708	0,233	0,239	0,472
6	12,783	140,067	0,227	0,244	0,471	12,108	148,244	0,250	0,230	0,480
7	12,855	141,007	0,230	0,241	0,471	11,914	151,948	0,238	0,233	0,471
8	12,636	142,657	0,228	0,248	0,476	12,607	145,239	0,219	0,246	0,465
9	12,337	142,962	0,229	0,243	0,473	12,772	140,802	0,220	0,246	0,467
10	12,746	135,864	0,223	0,253	0,477	11,371	146,979	0,270	0,227	0,497
11	12,665	143,138	0,240	0,242	0,482	13,977	132,083	0,206	0,259	0,465
12	13,765	132,719	0,206	0,258	0,464	11,990	152,816	0,237	0,229	0,466
13	12,413	140,034	0,230	0,247	0,477	11,856	147,911	0,246	0,234	0,480
14	12,577	144,348	0,236	0,240	0,476	13,265	131,913	0,210	0,253	0,463
15	12,438	141,000	0,233	0,246	0,479	11,801	146,527	0,255	0,228	0,483
16	12,492	143,903	0,233	0,238	0,471	12,412	141,784	0,233	0,247	0,480
17	12,665	137,454	0,227	0,249	0,477	13,639	139,530	0,208	0,249	0,458
18	12,361	138,502	0,235	0,244	0,480	12,778	139,956	0,230	0,239	0,469
19	13,539	135,379	0,212	0,258	0,469	12,598	138,116	0,229	0,248	0,477
20	12,204	147,404	0,235	0,246	0,480	12,500	138,512	0,231	0,249	0,480
21	12,311	142,288	0,232	0,245	0,476	12,865	136,117	0,229	0,252	0,481
22	12,556	141,590	0,231	0,243	0,473					
23	12,451	141,633	0,233	0,244	0,477					
24	12,683	132,916	0,235	0,259	0,494					
25	13,858	128,829	0,202	0,268	0,470					
26	13,460	131,222	0,215	0,258	0,472					
27	12,459	137,953	0,230	0,250	0,480					
28	13,214	133,501	0,220	0,258	0,477					
29	12,144	159,805	0,236	0,232	0,468					
30	12,563	135,515	0,228	0,253	0,481					
31	12,459	138,624	0,232	0,252	0,484					
32	11,911	143,691	0,240	0,243	0,482					
33	11,995	138,199	0,256	0,239	0,496					
34	12,315	140,584	0,232	0,246	0,478					
35	12,654	142,329	0,231	0,239	0,469					
36	13,778	130,052	0,210	0,266	0,476					
37	13,223	129,109	0,219	0,263	0,482					
38	12,885	135,440	0,221	0,253	0,473					
39	12,011	138,366	0,241	0,247	0,488					
40	13,801	133,601	0,207	0,254	0,461					
41	11,738	146,899	0,244	0,239	0,483					
42	13,062	136,646	0,219	0,250	0,468					

References

[1] Zhou, H., Pei, Y., Li, F., Luo, H. & Fang, D. *Appl. Phys. Lett* **2014,** 104, 061904.

[2] Abdollahi, A., Peco, C., Millán, D., Arroyo, M., Catalán, G. & Arias, I. *Phys. Rev B* **2015,** 92, 094101.

[3] Devonshire, A.F. *Phil. Mag* **1949,** 40, 1040.

[4] Zubko, P., Catalán, G. & Tagantsev, A.K. *Annu. Rev. Mater. Res.* **2013,** 43: 387 – 421.

[5] Sharma, N. D. , Landis C. M., and Sharma P., *J. Appl. Phys.* **2010,** 108: 024304.

[6] Shu L., Wei X., Pang T., Yao X. and Wang C. *J Appl Phys* **2011,** 110, 104106.

[7] Johnson K. L. *J Mech Phys Solids* **1970,** 18, 115–126.